MIXED-PHASE CLOUDS IN THE ARCTIC
A SYNOPSIS OF AIRBORNE LIDAR, IN-SITU, AND ALBEDOMETER OBSERVATIONS, COMPLEMENTED BY METEOROLOGICAL ANALYSES

Astrid Richter[1], Jean–François Gayet[2], Guillaume Mioche[2], André Ehrlich[3], Andreas Dörnbrack[4]

[1]*Alfred Wegener Institute for Polar and Marine Research, Telegrafenberg A43, D-14473 POTSDAM, Germany*
Astrid.Richter@awi.de
[2] *Laboratoire de Météorologie Physique UMR 6016 CNRS / Université Blaise Pascal, France.*
gayet@opgc.univ-bpclermont.fr, mioche@opgc.univ-bpclermont.fr
[3]*Johannes Gutenberg University Mainz, Institute for Atmospheric Physics, Becherweg21, D-55099 MAINZ, Germany,* ehrlichA@uni-mainz.de
[4]*Institut für Physik der Atmosphäre, DLR Oberpfaffenhofen, D-82230 WESSLING, Germany*
andreas.doernbrack@dlr.de

ABSTRACT

During the Arctic Study of Tropospheric Aerosol, Clouds and Radiation (ASTAR) 2007 campaign, airborne cloud observations were performed over the Arctic Ocean around Svalbard in the period from March till April 2007. On board of the AWI (Alfred Wegener Institute) Polar-2 aircraft, lidar remote sensing, *in-situ* cloud and albedometer solar radiation measurements were combined to investigate the properties of tropospheric clouds in the Arctic. On April 8th, a mixed-phase cloud formation was observed in a cold-air outbreak over open water. On April 9th, mixed-phase clouds were probed in two different air masses. First we observed remnants of the northerly cold-air outbreak which was gradually replaced by warmer air originating from the South. In the mixing zone between both air masses, the cloud consisted of pure ice.

1. INTRODUCTION

Generally, clouds play a crucial role in the energy budget of the Arctic atmosphere. Sensitive feedback mechanisms include interaction with the high surface albedo, aerosol, radiation, cloud water content, and cloud drop size [1]. Especially the impacts of Arctic tropospheric mixed-phase clouds are difficult to predict by current weather and climate models [2]. Therefore, observational data are needed to further understand the radiative effects of these clouds and to achieve suitable parameterizations in numerical prediction models.

In the spirit of the predecessor campaigns in 2000 [3] and 2004 [4], the ASTAR 2007 campaign investigated tropospheric processes and interactions of aerosol, clouds and radiation during Arctic springtime conditions. Two research aircraft operating from Longyearbyen airport, the AWI Polar-2 (Do228) and the DLR Falcon, participated with unique and complementary instruments. The ambient weather conditions during most parts of the campaign were characterized by prevailing northerly or north-easterly flows associated with clean Arctic air near Svalbard.

The explicit aim of the research flight on 8th April was to investigate the properties of boundary layer clouds forming in a cold air outbreak west of Svalbard. Along a flight track, nearly perpendicular to the longitudinal convective roll clouds, we probed the clouds by deploying the *in-situ* instrumentation. Along the same flight track backward, we performed simultaneous remote-sensing measurements with lidar and solar radiation sensors at an altitude of 2730 m.

The flight on 9th April was planned as a contribution to the CALIPSO and CloudSat satellite validation project. Running the remote-sensing configuration, Polar-2 followed the footprint of the satellite track at an altitude of 2700 m toward North-West nearly synchronously. Reaching the predefined northernmost waypoint, the aircraft turned and flew back the same path descending and ascending from cloud top to cloud bottom deploying the *in-situ* sensors. The actual coincidence with the satellite overpass occurred on the way back during the *in-situ* measurements.

2. INSTRUMENTATION

The instrumentation on board of the AWI Polar-2 aircraft consisted of standard meteorological sensors (pressure, temperature, humidity, wind), the Airborne Mobile Aerosol Lidar (AMALi), the SMART-Albedometer (Spectral Modular Airborne Radiation measurement sysTem), and the *in-situ* instruments Polar Nephelometer, CPI (Cloud Particle Imager), and PMS-FSSP (Particle Measuring System, Forward Scattering Spectrometer Probe).

The AMALi is a 2-wavelength (532 nm and 355 nm; recently, 1064 nm was exchanged against 355 nm) backscatter lidar with depolarization measurements at

532 nm, operated by AWI. In this paper, only the signal at 532 nm in both polarizations is further considered. For cloud particles with large diameters compared to the wavelength, not much additional information can be retrieved from the second wavelength at 355 nm. The vertical resolution amounts to 7.5 m. For the cases discussed here, AMALi was installed in nadir looking configuration. Further details of AMALi's technical properties can be found in [5]. The minimum horizontal resolution, determined by an acceptable signal to noise ratio (above 20) and the aircraft's groundspeed of about 60 m/s, was around 900 m.

The different *in-situ* instruments were operated by the Laboratoire de Météorologie Physique (LaMP). They provided independent measurements of particle concentration, extinction coefficient, ice and liquid water content, effective diameter, phase function and asymmetry parameter. The instruments and data retrieval are described in [6].

The SMART-Albedometer operated by the University of Mainz measures downwelling irradiance $F^{\downarrow}_{\lambda}$ and upwelling nadir radiance $L^{\uparrow}_{\lambda}$ in the visible (350-1000 nm) and near-infrared range (1000-2100 nm) and is actively horizontally stabilized for airborne applications [7]. From the measurements spectral cloud top reflectance $R_{\lambda}=\pi L^{\uparrow}_{\lambda}/F^{\downarrow}_{\lambda}$ was calculated and analyzed with the ice index

$$S_I = 100 \cdot (R_{1700nm} - R_{1550nm}) / R_{1640nm}, \qquad (1)$$

according to Knap [8] using an extended wavelength range of 1550-1700 nm. S_I is a suitable criterion for cloud phase discrimination.

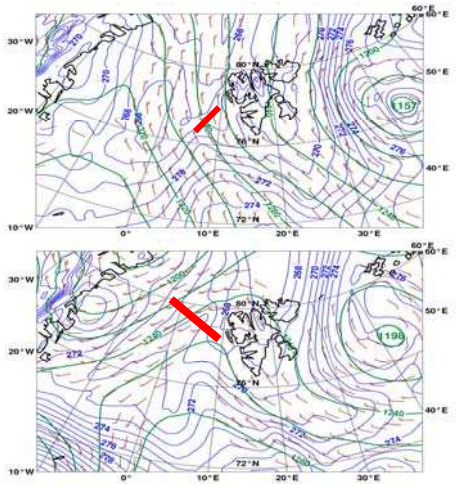

Figure 1: Geopotential height (m, green lines), equivalent potential temperature (K, blue lines) and wind speed (ms^{-1}, barbs) at 850 hPa on 8th April (top) and 9th April 2007 (bottom) at 12 UTC. The approximate locations of the flight paths are indicated by red lines. Meteorological data are taken from operational ECMWF analyses.

3. METEOROLOGICAL EVOLUTION

On the back of a slowly north-eastward propagating trough, cold air was ejected from higher latitudes towards Svalbard on 8th April 2007 (see Fig. 1). This cold-air outbreak was associated with cloud streets consisting of convective roll clouds forming south of the ice edge and extending far south (see Fig. 2). On 9th April 2007, a ridge built up west of Svalbard and disrupted the cold air outflow. After the passage of the ridge axis, warmer and moister tropospheric air from the South replaced the cold air masses from the North.

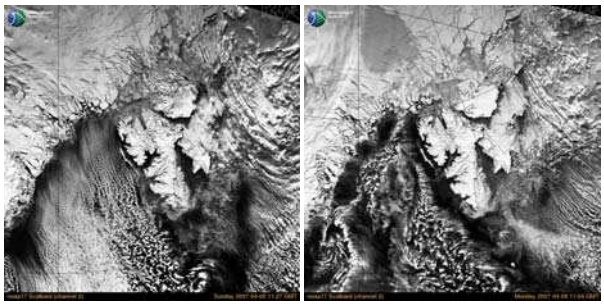

Figure 2: NOAA visible satellite imagery on 8th April 2007 1127 UTC (left panel) and 9th April 2007 1104 UTC (right panel).

4. LIDAR, IN SITU AND ALBEDOMETER MEASUREMENTS

4.1 8th April 2007

On 8th April 2007, a sequence of lidar backscatter profiles (Fig. 3) depicts the cloud top of boundary layer clouds extending up to an altitude of 1600 m.

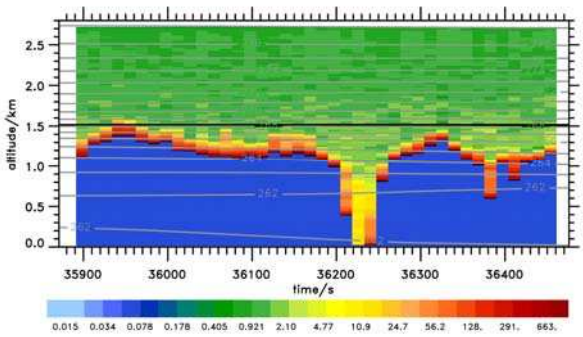

Figure 3: Lidar backscatter ratio (color shaded) along the flight track on 8th April 2007. Potential temperature (K, grey lines) interpolated in time and space on the flight track. The straight black line indicates the boundary layer height (see text). Meteorological data are taken from operational ECMWF analyses.

The upper edge of this low-level cloud layer shows wavelike undulations. As the clouds were forming in a cold-air outbreak over the warmer water, it is most likely that these undulations are the signature of

convective roll clouds. This argument is supported by the low static stability $N^2 = g/\Theta_0 \, \partial\Theta/\partial z$ in the near adiabatic boundary layer underneath a sharp inversion as seen by the broadly spaced isentropic surfaces from the operational ECMWF analyses, see Fig. 3. However, the ECMWF analyses cannot resolve the mesoscale features of the convective clouds and give a uniform boundary layer height of about 1500 m. This height was determined as the height of maximum N^2 (inversion) which here coincides with a local maximum of the potential vorticity attaining a nearly stratospheric value of 1.9 PVU.

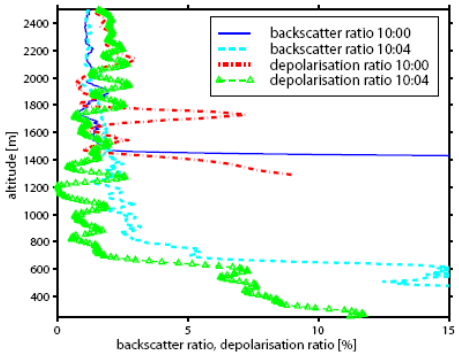

Figure 4: Vertical profiles of backscatter ratio and volume depolarization for the mixed-phase clouds on 8th April 2007: 10:00 UTC thick water layer on cloud top, 10:04 UTC cloud gap with ice precipitation detected near the surface.

The strong backscatter ratio together with the low volume depolarization at the cloud top (1500 m), increasing gradually with range (Fig. 4), indicate a liquid water layer on cloud top and multiple scattering effects [9]. The clouds were optically too thick and attenuated the laser beam significantly, thus they did not allow lidar measurements down to the sea surface. Only in a cloud gap at around 10:04 UTC (~36250 s in Fig. 3), the lidar was able to penetrate to the surface and detected the ice particle signature, high depolarization and low backscatter, in the lowest 700 m (Fig. 4).

Generally, the simultaneously performed cloud top reflection measurements showed the existence of mixed-phase clouds which were clearly dominated by water. The spectral pattern of the cloud reflectance in the range 1550 – 1700 nm affected by ice and water absorption resulted in an average ice index of S_I= 23 for the mixed-phase clouds observed on 8th April (S_I = 10 corresponds to pure water, S_I = 50-60 to pure ice clouds).

The vertical profiles of the *in-situ* measurements demonstrated a 500 m thick layer of pure liquid water droplets and below ice particles (not shown).

4.2 9th April 2007

On 9th April 2007, the aerosol backscatter ratio as shown in Fig. 5 reveals a gradual increase of the cloud top height along the flight track. This observation agrees with the superimposed isentropic surfaces which indicate an increase of the boundary layer depth along the flight track. Here, we calculated the boundary layer height as the location of maximum N^2 or as the minimum altitude where $N > 0.015$ s^{-1}. At about 09:00 UTC (32500 s in Fig. 5), the continuous cloud layer broke up and scattered clouds were detected. In contrast to the continuous cloud deck, the lidar signal could penetrate these clouds almost completely throughout their depth.

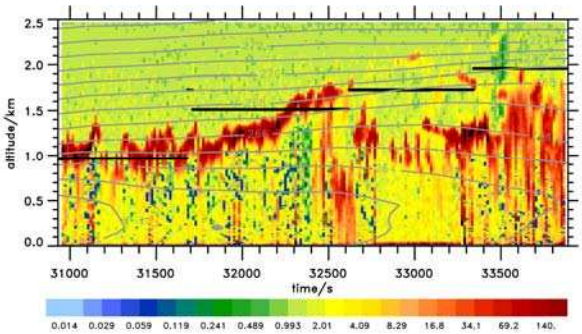

Figure 5: Lidar backscatter ratio (color shaded) along the flight track toward NW on 9th April. Potential temperature (K, grey lines) interpolated in time and space on the flight track. The straight black lines indicate the boundary layer height (see text). Meteorological data are taken from operational ECMWF analyses.

This finding points to different processes of cloud evolution. In fact, the meteorological analyses reveal that the lidar sampled air masses of different origin: During the first part of the research flight, we observed remnants of the northerly cold-air outbreak which was gradually replaced by warmer air originating from the South.

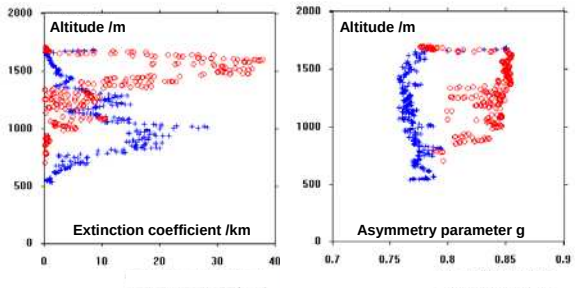

Figure 6: Vertical profiles of in situ measurements on 9th April 2007: Red circles are observations of extinction coefficient (left) and asymmetry parameter (right) in the water cloud, blue crosses represent measurements in the pure ice part of the cloud.

Depolarization measurements generally showed the same cloud features. But the values of depolarization were only slightly enhanced. So either areas of ice particles smaller than the lidar horizontal resolution were present or this was an effect of multiple scattering. On two occasions, however, the depolarization signal was clearly enhanced (above 20%) while the backscatter signal was comparatively low, which gives evidence of ice particles.

The ice index calculated from measured spectral cloud top reflectance was almost constant for the entire flight leg with $S_I = 18.5$. Two exceptions with ice index up to 60 were observed, indicating pure ice clouds below the aircraft at 09:01 and 09:20 UTC.

The *in-situ* measurements found mostly water droplets for the upper 700 m (asymmetry parameter higher than 0.8) and ice particles below (asymmetry parameter smaller than 0.8). However, considerable ice content with an extinction coefficient up to 20 was recorded in the pure ice cloud observed in the mixing zone (Fig. 6).

5. ANALYSIS AND COMPARISON

Qualitatively, the identification of cloud phase of all three instruments agreed, even with the time delay between the *in-situ* and remote measurements. Advection of the sampled air masses was taken into account for comparison.

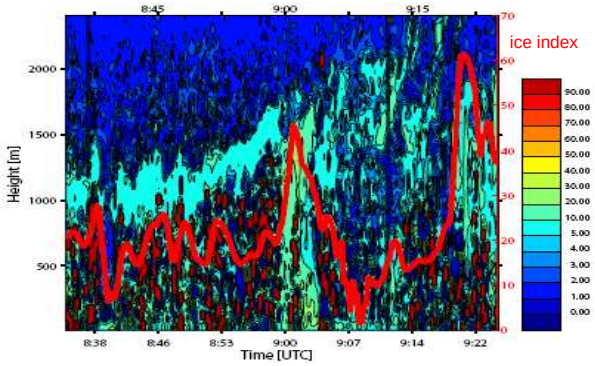

Figure 7: Lidar volume depolarization [%] (color shaded) along the flight track toward NW on 9th April 2007. Superimposed (red line) is the ice index calculated from albedometer data measured simultaneously.

The cloud system on 8th April was capped with a geometrically and optically thick water layer. Only once during the flight leg, the lidar detected ice precipitation in a cloud gap. The *in-situ* measurements were not performed near the ground, so no significant ice crystal precipitation was observed. The clouds on 9th April showed an interesting feature along the mixing zone of the 2 different air masses (cold air from the North, warmer airmass advected from the South-West): both the enhanced lidar depolarization and the higher ice index showed the existence of a pure ice cloud (Fig. 7). *In-situ* measurements were performed around 30 minutes later. Due to advection, we were not able to probe the cloud at the same intersection again. But a pure ice cloud was equally found at the mixing zone.

6. CONCLUSIONS

Combining lidar vertical profiling, solar radiation measurements and *in-situ* observations, we were able to observe small- and mesoscale features of Arctic mixed-phase clouds. This promising ensemble of instruments gave a complete picture of the spatial distribution, optical and microphysical properties and radiative effects, and will allow further studies to investigate directly the mechanisms of cloud radiative forcing.

REFERENCES

[1] Curry, J.A., Rossow, W.B., Randall, D., Schramm, J.L., 1996: Overview of Arctic Cloud and Radiation Characteristics, *Journal of Climate*, **9**, pp. 1731-1764.

[2] Inoue, J., Liu, J., Pinto, J.O., Curry, J.A., 2006: Intercomparison of Arctic Regional Climate Models: Modeling Clouds and Radiation for SHEBA in May 1998, Journal of Climate, 19, pp. 4167-4178.

[3] Treffeisen, R., Rinke, A., Fortmann, M., Dethloff, K., Herber, A., Yamanouchi, T., 2005: An estimation on the radiative effects of Arctic aerosols using two different aerosol data sets: A case study for March 2000, *Atmos. Environm.*, **39**, pp. 887-899.

[4] Engvall, A.-C., Krejci, R., Ström, J., Minikin, A., Treffeisen, R., Stohl, A., Herber, A., 2008: In-situ airborne observations of the microphysical properties of the Arctic tropospheric aerosol during late spring and summer, accepted to Tellus B.

[5] Stachlewska, I.S., Wehrle, G., Stein, B., Neuber, R., 2004: Airborne Mobile Aerosol Lidar for measurements of Arctic aerosols, *Proceedings of 22nd International Laser Radar Conference (ILRC2004), ESA SP-561,* **1**, pp. 87-89.

[6] Gayet J.-F., Stachlewska, I.S., Jourdan, O., Shcherbakov, V., Schwarzenboeck, A., Neuber, R., 2007: Microphysical and optical properties of precipitating drizzle and ice particles obtained from alternated Lidar and in situ measurements. *Annales Geophys*., **25**, 1487-1497.

[7] Wendisch, M., Müller, D., Schell, D., Heintzenberg, J., 2001: An airborne spectral albedometer with active horizontal stabilization, *J. Atmos. Oceanic Technol*., **18**, 1856– 1866.

[8] Knap, W., Stammes, P., and Koelemeijer, R., 2002: Cloud thermodynamic-phase determination from near-infrared spectra of reflected sunlight, *J. Atmos. Sci*., **59**, 83–96.

[9] Hu, Y., Vaughan, M., Liu, Z., Lin, B., Yang, P., Flittner, D., Hunt, B., Kuehn, R., Huang, J., Wu, D., Rodier, S., Powell, K., Trepte, C., Winker, D., 2007: The depolarization – attenuated backscatter relation: CALIPSO lidar measurements vs. theory, Optics Express, 15,9, pp. 5327-5332.